NEURO

CrossMark

Machine learning identifies "rsfMRI epilepsy networks" in temporal lobe epilepsy

Rose Dawn Bharath [1,2] · Rajanikant Panda [1,2,3] · Jeetu Raj [4] · Sujas Bhardwaj [1,2,5] · Sanjib Sinha [5] · Ganne Chaitanya [5,6] ·
Kenchaiah Raghavendra [5] · Ravindranadh C. Mundlamuri [5] · Arivazhagan Arimappamagan [7] · Malla Bhaskara Rao [7] ·
Jamuna Rajeshwaran [8] · Kandavel Thennarasu [9] · Kaushik K. Majumdar [10] · Parthasarthy Satishchandra [7] ·
Tapan K. Gandhi [11]

Abstract

Objectives Experimental models have provided compelling evidence for the existence of neural networks in temporal lobe epilepsy (TLE). To identify and validate the possible existence of resting-state "epilepsy networks," we used machine learning methods on resting-state functional magnetic resonance imaging (rsfMRI) data from 42 individuals with TLE.
Methods Probabilistic independent component analysis (PICA) was applied to rsfMRI data from 132 subjects (42 TLE patients + 90 healthy controls) and 88 independent components (ICs) were obtained following standard procedures. Elastic net-selected features were used as inputs to support vector machine (SVM). The strengths of the top 10 networks were correlated with clinical features to obtain "rsfMRI epilepsy networks."
Results SVM could classify individuals with epilepsy with 97.5% accuracy (sensitivity = 100%, specificity = 94.4%). Ten networks with the highest ranking were found in the frontal, perisylvian, cingulo-insular, posterior-quadrant, thalamic, cerebello-thalamic, and temporo-thalamic regions. The posterior-quadrant, cerebello-thalamic, thalamic, medial-visual, and perisylvian networks revealed significant correlation ($r > 0.40$) with age at onset of seizures, the frequency of seizures, duration of illness, and a number of anti-epileptic drugs.
Conclusions IC-derived rsfMRI networks contain epilepsy-related networks and machine learning methods are useful in identifying these networks in vivo. Increased network strength with disease progression in these "rsfMRI epilepsy networks" could reflect epileptogenesis in TLE.

Key Points
• *ICA of resting-state fMRI carries disease-specific information about epilepsy.*
• *Machine learning can classify these components with 97.5% accuracy.*
• *"Subject-specific epilepsy networks" could quantify "epileptogenesis" in vivo.*

Keywords Temporal lobe epilepsy · Magnetic resonance imaging · Support vector machine · Seizures

Abbreviations

CA1-CA4	Cornus amonis
FD	Fascia dentata
FDR	False discovery rate
HGMV	Hippocampal gray matter volume
ICA	Independent component analysis
ICs	Independent components
ML	Machine learning
MTS	Mesial temporal sclerosis
PICA	Probabilistic independent component analysis
ROI	Region of interest
rsfMRI	Resting-state functional magnetic resonance imaging
SUB	Subiculum
SVM	Support vector machine
TLE	Temporal lobe epilepsy

✉ Tapan K. Gandhi
cns.researchers1@gmail.com; gandhitk@gmail.com

Extended author information available on the last page of the article

Introduction

Volumetric imaging studies have corroborated the increasing evidence that temporal lobe epilepsy (TLE) is a network disorder and extends beyond the evident hippocampal atrophy and signal changes in a patient with mesial temporal sclerosis (MTS). Whole brain network analysis using graph theoretical methods has further intensified the evidence and has allowed in vivo imaging of its pathophysiology [1]. Network abnormalities probably reflecting the combination of the disease process and compensatory plasticity response are noted in frontal, parietal, and occipital lobes [2, 3]. Independent component analysis (ICA), another data-driven whole brain network analysis of resting-state functional magnetic resonance imaging (rsfMRI), has also provided evidence for widespread network alterations, involving default mode network [4, 5], auditory, sensorimotor, visual [6], language [7], basal ganglia, and cerebellum networks [8] in patients with epilepsy. Though ICA derives 15–80 components, rsfMRI research typically focuses on 10 well-identified networks, namely sensorimotor, visual, auditory, default-mode, attention, salience, executive, basal ganglia, and cerebellar networks. One of the main reasons why remaining components are not used is because their spatial structure is not pertinent to our concept of brain function as defined by task-based fMRI [9]. With the availability of probabilistic ICA (PICA) methods, the accuracy and efficiency of modeling noise [10] and extracting signals of interest in the spatiotemporal and subject-session domain in multisubject/multisession fMRI data [10–14] have created a renewed interest in these less popular components. In addition, EEG-fMRI studies also have reported physiological correlations with mathematically eliminated global signal [15] and spike-wave discharges have revealed spatial and temporal correlations with these components [16]. It is possible that epilepsy could reveal disease proportionate changes within these discarded components and allow us to measure disease progression.

Machine learning (ML) is an application of artificial intelligence that allows computers to learn from the data in hand without being explicitly programmed [17]. ML has found critical clinical applications in better understanding complex multi-factorial diseases by establishing a diagnosis [18], measuring disease progression [19], detecting high-risk healthy subjects, and even predicting survival [20]. The fundamental building block in ML is a "neuron" with an input and output function strikingly similar to the structure of the human unipolar neuron. Based on the extent of learning, these algorithms can be broadly divided into supervised learning and unsupervised learning. Support vector machine (SVM) is a popular supervised learning technique because of its power to deal with complex nonlinear data [18]. One critical aspect in ML is the suitable feature selection. Prior studies have used features like task-based functional connectivity, ROI-based resting functional connectivity [21], and independent component analysis (ICA)–derived resting networks [22] as input features. In recent trends, ML algorithms can extract the weight of every feature in a set of features used for the data classification by a process called "feature ranking." Some popular algorithms used for this task are sparse logistic regression, lasso, kernel ridge regression, Bayesian regularization, elastic net regression, etc. Over these, elastic net is one of the efficient algorithms for feature selection in neuroimaging data [23–25].

With an aim to characterize ICs that could be indicative of TLE, we undertook this exploratory study using 88 ICA-derived resting networks as inputs to one of the most popular ML algorithms, SVM. We hypothesized that there could be "disease-specific IC networks" (reflective of the alterations in the epileptogenic brain), that can be correctly identified with the help of the ML model. Elastic net-based ranking was used to characterize these networks on the basis of their anatomical structure and also on disease-defining clinical variables like age at onset of disease, the frequency of seizure, number of anti-epileptic drugs, etc. This ranking was critical for us to link ICs with disease progression.

Materials and methods

Participants

The study was conducted in a tertiary neurological institute in patients referred for imaging evaluation for refractory TLE following approval of the institute ethics committee and written informed consent. Forty-two TLE patients (male:female, 27:15; mean age, 24 ± 7.9 years) with 11.8 ± 7.4 years of age at onset of disease and 12 ± 6.4-year duration of illness, having a mean seizure frequency of 5.6 ± 8.4 per month, were recruited in the interictal period. Structural MRI (RDB) and scalp EEG (GC/PSC/SS) were verified and 18 patients had right mesial temporal sclerosis (MTS), 19 left MTS, and 5 bilateral MTS. All patients were on poly-pharmacy on levetiracetam, valproate, phenytoin, carbamazepine, etc. (22 patients were on two drugs, 16 on three, and 4 on more than three drugs). For the control group, data of 90 age- and gender-matched (M:F = 53:37; age, 26.7 ± 10.2 years) subjects were selected from the existing healthy-subject imaging data bank.

Image acquisition

Patients underwent rsfMRI thrice in succession and controls once (185 dynamics; TR/TE/FA: 3000 ms, 30 ms, 90°, 34 slices, 64×64, $3 \times 3 \times 4$ mm). Hence, the total acquired data were 216 (126 patient data and 90 controls). All subjects had one T1-MPRAGE (TR/TE/FA, 1900 ms, 2.43 ms, 90° and ST, 1 mm) in a 3T MRI (Skyra-Siemens).

Data analysis

Independent components

Preprocessing was done using FSL (FMRIB's Software Library) following brain extraction, motion correction, spatial smoothing, intensity normalization and band-pass filtering, co-registration with structural volume in MNI152, and resampling of the filtered data into standard space [26]. Fourteen data sets were discarded due to head motion. ICs were analyzed with probabilistic independent component analysis (PICA). ICs were extracted and visually inspected at individual subject level. The ICs having obvious non-physiological activity were discarded. Multivariate group PICA was carried out to derive temporally concatenated maximal spatially ICs across the 202 data sets (90 controls and 112 patient data). Decomposition of the data set into 88 independent vectors was performed through automated data specific IC decomposition using the Fast ICA algorithm [26]. To extract the individual ICs and to test for group-wise comparisons, dual regression was performed. The set of spatial maps derived from the group-mean analysis was used to generate individual subject-specific spatial maps and their time series [27]. Statistical analysis was done using a randomized, non-parametric permutation, adapting the threshold-free cluster enhancement (TFCE) technique at $p < 0.05$ threshold.

Feature set construction and selection

The feature set was composed of a Pearson's correlation matrix created from the time courses corresponding to ICs. Taking all 88-time series corresponding to each IC and picking up the upper triangular region and unraveling it into a vector we obtained a feature vector of dimension 3828. We opted for elastic net [28] for feature selection among all candidates.

Elastic net is a regularized linear regression model which includes two kinds of regularizes such as L1 and L2. L1 regularizer allows learning weights for features, which are sparse in nature while L2 regulates their magnitude.

$$O(X) = \text{argmin}_W |Y - XW|^2 + \lambda_1 |W| + \lambda_2 |W|^2$$

"Y" is the label of categories (i.e., patient or healthy control), "W" is the weight of the matrix, λ_1 is the coefficient of l1 regularize, and λ_2 is the coefficient of l1 regularize. The above functions find the loss function, which consists of mean squared loss along with two regularizer terms. Elastic net learns weights for features, which are sparse in nature facilitating the selection of features by picking features which have non-zero weights. Mathematically describing:

$$I_{\text{selected}} = \{i \in I \,|\, W_i > 0\}$$

I is the set of indexes in features where I_{selected} selected set of indexes [1]. In order to rank a region, the weights corresponding to the correlation features with respect to all other region are taken. A region is ranked higher if it has in general higher aggregated feature weights indicating its importance. Rankings for different regions are obtained as follows:

$$R_i = \sum_{j \in \{0, \text{cols}_M\}} W_{ij}$$

where M_{ij} is the correlation feature between ith and jth region, then W_{ij} is the weight assigned by elastic net to M_{ij}, and R_i is the score based on which ith region is ranked [1].

The superiority of elastic net over other techniques such as lasso and sparse canonical correlation analysis is highlighted in an article of Zou et al [29].

It consists of a mean square cost function along with l_1 (sparsity) and l_2 (smoothness) regularizers for the weights shown above in the equation with α being the coefficient of the l_1 term and β for the l_2 term. X is the training data matrix and Y is the set of labels with weights. The model leads to a sparse weight vector which is used to select features. All features with positive weights were picked while the rest were dropped. The resulting feature vector was of dimension 187 which was comparable to the count of data-points. α was kept at 0.0075 to ensure sufficient sparsity and β at 0.021.

Data classification

For classification pattern recognition, model "linear SVM" was employed. Two class SVM was trained with its penalty parameter set to 1.0 using Sklearn library in python.

Ranking of independent components

The elastic net feature selection step provided a weight for each correlation feature and by summing up the weights for the correlations for a particular IC, we could obtain a score for each IC. The coefficient of regressor was also reduced to 0.0035 as the original feature dimension was also reduced.

This approach can be interpreted in another fashion in the form of a graph. In this, the ICs represent the nodes and a pair of ICs has an edge between them if their correlation feature has a positive weight obtained from the elastic net. This weight represents the edge weight leading to a weighted undirected graph. Ranking of ICs is based on the degree centrality measure for weighted graphs [30].

Hippocampal volume calculation

Hippocampal gray matter volume (HGMV) was calculated using (HV-SPM8) toolbox (https://www.fil.ion.ucl.ac.uk/spm/ext/#HV) following Suppa et al [31]. This toolbox allows fully

automated tissue segmentation and stereotactical normalization of high-resolution 3D MPRAGE images. To calculate HGMV, we included cornus amonis (CA1-CA4), fascia dentata (FD), and subiculum (SUB). HGMV was calculated by multiplying the subject's GM component image with a predefined binary mask from atlas [32] adding all voxel intensities.

Clinical correlation

The strength of the ICs which showed the top 10 ranking in predicting TLE was correlated with various clinical features and hippocampal volume using Pearson's correlation. To calculate the strength of ICs, the effect size was calculated by taking the sum of the intensity of all clusters divided by the total number of voxels in the network. Correction for multiple comparisons was done using false discovery rate (FDR), $p < 0.01$.

Results

ML identified 10 ICs in TLE patients capable of predicting epilepsy with an accuracy of 97.5% with fivefold cross-validation. These ICs involved frontal, temporal, perisylvian, cingulate, posterior-quadrant, thalamic, and cerebellar regions. The strength of some of these networks was proportional to clinical variables.

Classification of patients with TLE

As evident in Table 1, the SVM algorithm produced 97.5% accuracy and correctly identified all patient trials with epilepsy, while interpreting 5 out of 90 healthy controls as having epilepsy.

Elastic net ranking of independent components

Elastic net-based top 10 networks were IC12, IC10, IC22, IC3, IC18, IC15, IC23, IC19, IC25, and IC32 in descending order of their significance.

Spatial correlation of these networks [33] revealed that these networks matched the 70 component template more than 25%. The networks and their correlations are provided in Table 2.

Table 1 SVM classification model

Model	SEN	SPE	PPV	NPV	ACC
SVM	100	94.4	95.72	100	97.52

SEN classification sensitivity, *SPE* classification specificity, *PPV* positive predictive values, *NPV* negative predictive values, *ACC* classification accuracy

Structural anatomy of top 10 independent components

The regions and their coordinates in the order of their ranks are presented in Fig. 1 and supplementary Table 1.

Rank1: IC12: involved the posterior quadrant including posterior temporal, occipital, and parietal lobes bilaterally.

Rank2: IC10: involved the posterior temporal and occipital lobes bilaterally.

Rank3: IC22: predominantly involved the orbitofrontal, lateral frontal, cingulate, and anterior insula bilaterally.

Rank4: IC3: had dense involvement of the cerebellum, vermis, brain stem, and medial thalamus bilaterally.

Rank5: IC18: involved the entire cingulate gyrus and anterior insula bilaterally.

Rank6: IC15: involved the entire thalamus bilaterally without involving the brain stem.

Rank7: IC23: involved the medial occipital lobes bilaterally.

Rank8: IC19: involved the insula and perisylvian region bilaterally with anterior cingulate gyrus.

Rank9: IC25: involved the superior and middle frontal gyrus bilaterally.

Rank10: IC32: involved the antero-medial temporal lobes, brain stem, and thalamus bilaterally.

Clinical correlation

Since the frequency of seizures ranged from 0.3 to 50, five patients with a frequency higher than 8 (> 2 SD) were excluded from the correlation analysis (Fig. 2, Table 3). The posterior-quadrant network (IC12) correlated positively with the duration of epilepsy ($r = 0.58$) and the number of antiepileptic drugs ($r = 0.41$). The cerebello-thalamic network (IC03) correlated negatively ($r = -0.48$) with the age at onset of seizures. The thalamic network (IC15) correlated positively with the duration of epilepsy ($r = 0.48$). The medial-visual network (IC23) correlated negatively with the age at onset of seizures ($r = -0.53$). The perisylvian network (IC19) correlated positively with the frequency of seizures ($r = 0.72$).

Hippocampal volume correlation

For the purpose of correlation, we classified hippocampus into the affected and unaffected sides. For example, the right hippocampus in patients with right MTS was classified as affected and the left hippocampus in the same patient was classified unaffected. In patients with bilateral MTS, both hippocampi were classified affected. We found a significant correlation (< 0.05 FDR) between affected hippocampus with rank 1(IC 12) network ($r = -38$, $p = 3.02e{-}05$) and rank 10 (IC 32) network ($r = -45$, $p = 3.87e{-}07$) (Fig. 3). Unaffected hippocampal volume did not correlate with the network strength.

Table 2 Elastic net-derived networks

Ranks	Epilepsy networks	20 component ICA template		70 component ICA template	
		Template IC	r value	Template IC	r value
1	IC12	10_{20}	0.28	11_{70}	0.39
2	IC10	10_{20}	0.61	25_{70}	0.54
3	IC22	8_{20}	0.40	43_{70}	0.42
4	IC3	9_{20}	0.48	4_{70}	0.36
5	IC18	8_{20}	0.46	7_{70}	0.29
6	IC15	$8_{20}, 4_{20}$	0.29	8_{70}	0.59
7	IC23	6_{20}	0.33	54_{70}	0.41
8	IC19	3_{20}	0.36	16_{70}	0.39
9	IC25	11_{20}	0.27	22_{70}	0.30
10	IC32	4_{20}	0.26	40_{70}	0.56

Discussion

The study provides a novel proof of concept evidence for the existence of "rsfMRI epilepsy networks" in patients with TLE. Powerful ML algorithm like SVM identified these ICs with 100% sensitivity and 97.5% accuracy, providing initial and crucial evidence for the possible existence of these disease-specific networks. The spatial organization of networks in the fronto-polar, cingulo-insular, perisylvian, posterior quadrant, cerebello-thalamic, and temporo-thalamic areas provided additional evidence for their existence as these areas have been strongly implicated in temporal plus syndrome [34]. Another
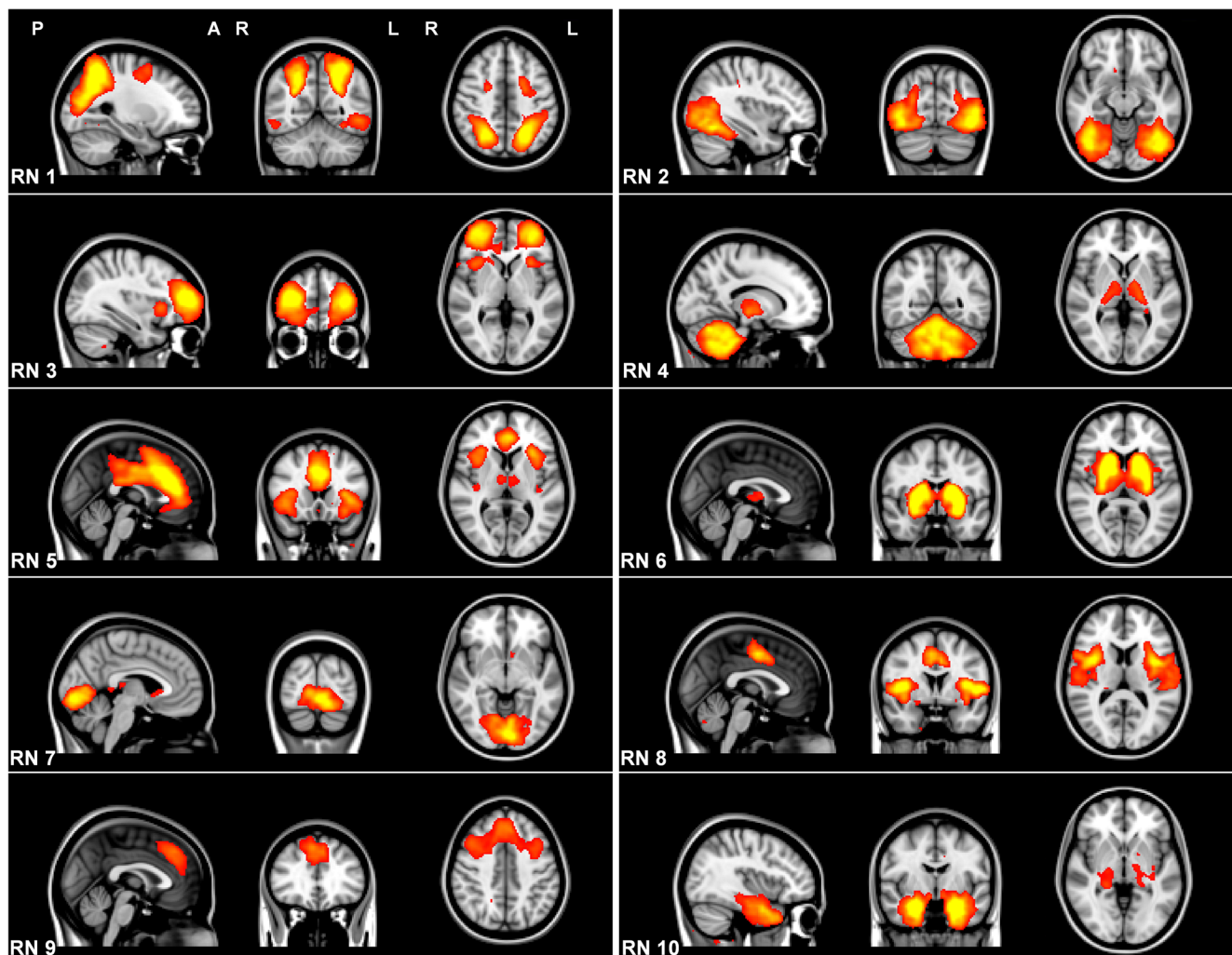

Fig. 1 The spatial maps of the top 10 networks identified through elastic net which identified patients living with epilepsy most accurately. This figure shows the most informative orthogonal slices of each network ranked from 1 to 10
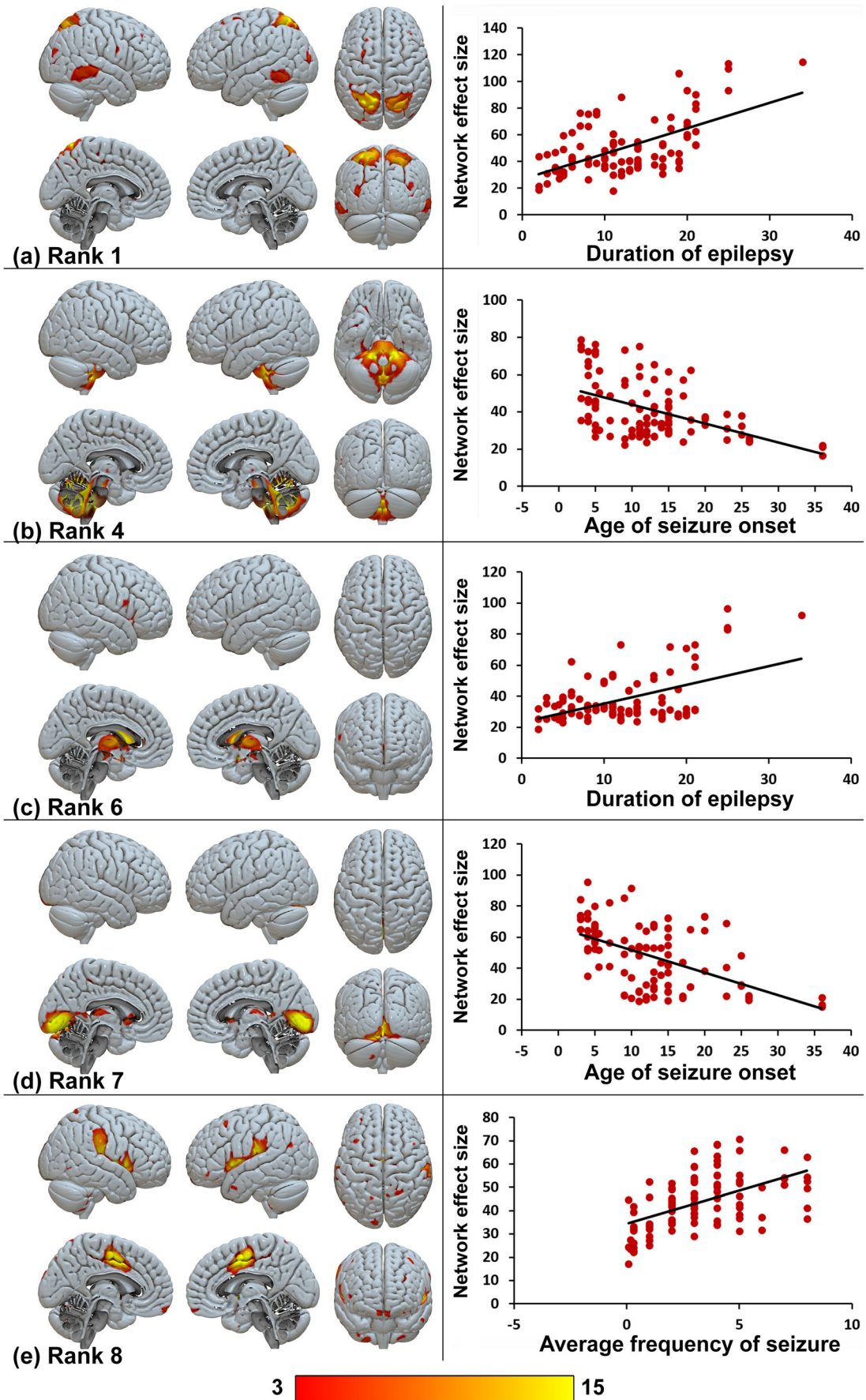
◄ **Fig. 2** Clinical correlations of the networks. IC12 (rank 1), IC03 (rank 4), IC15 (rank 6), IC23 (rank 7), and IC19 (rank 8) increased in their network strength with duration of disease, the frequency of seizures and to a younger age at onset of disease

important indication for their existence came from the survival of contemporary noise correction methods and having > 25% correlation with the IC_{70} template indicating that these ICs could not have been noise. We employed labor intensive but gold standard [35] hand classification of components in each and every patient; this step was critical for differentiating "epilepsy networks" from noise [36]. Several known pitfalls while using ML methods [18] were carefully addressed, with validation through fivefold stratified cross-validation, reporting of the entire confusion matrix of results, relatively larger sample size with 202 data sets and the fact that the individuals who actually performed the analysis (RP, TG, and JRaj) were blind to the clinical relevance of these networks. However, the conclusive evidence for their existence has come from the significant correlation of networks with disease-defining clinical features and diseased hippocampal volume.

Though there are no prior reports on IC-based "rsfMRI epilepsy networks," the existence of disease-specific metabolic networks is known with FDG-PET using spatial covariance analysis techniques. Such disease-specific metabolic networks subordinating healthy networks and strengthening with disease progression have been observed in Parkinson's disease [37]. Prior studies have provided evidence for epilepsy subordinating resting networks in patients with epilepsy [4–8]. Significant correlations with cognitive scores [6] also support cognitive deficits associated alterations of rsfMRI networks. From the current results, we can only infer that these networks are significantly associated with epilepsy. We cannot differentiate networks subordinated by disease, drugs, and cognitive deficits from disease-specific networks. Nevertheless, it is compelling to note the significant ($p < 0.05$ FDR) negative correlation of IC 12 and 32 with
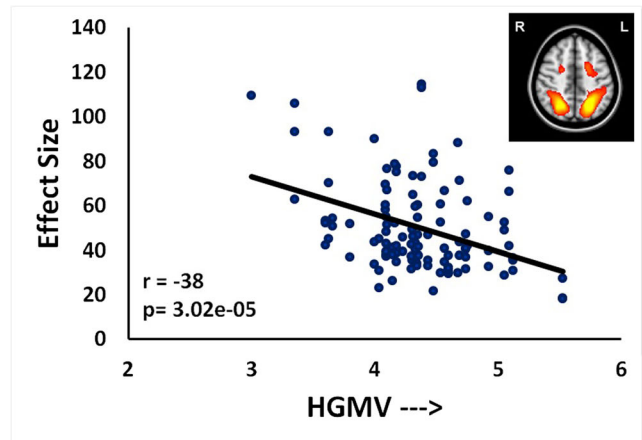
(a) Rank 1
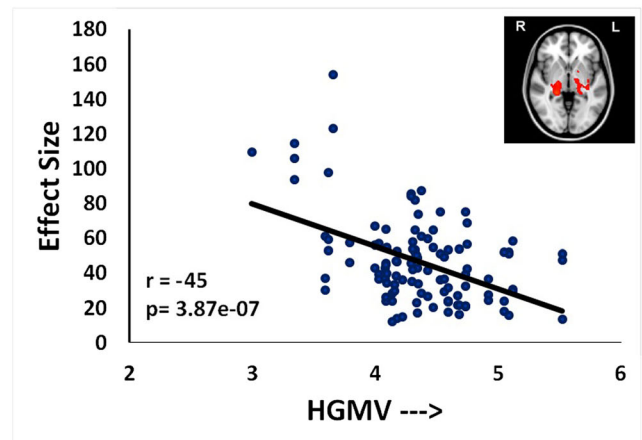
(b) Rank 10

Fig. 3 Affected hippocampal volume correlation with effect size of ICs. **a** Rank 1. **b** Rank 10

hippocampal volume and the positive correlation of IC 12, 3, 15, 23, and 19 with the clinical variables like age at onset, duration of epilepsy, frequency of seizures, and number of anti-

Table 3 Clinical correlation of networks

Ranks	Epilepsy networks	Anatomical regions	Age of seizure onset		Duration of epilepsy		Average frequency of seizures		No. of anti-epileptic drugs	
			r value	p value	r value	p value	r value	p value	r value	p value
1	IC12	Posterior quadrant	− 0.23	0.01	0.58	2.32e−10*	− 0.01	0.85	0.41	0.00001*
2	IC10	Lateral visual	− 0.07	0.44	0.01	0.91	− 0.09	0.34	− 0.01	0.89
3	IC22	Frontopolar	− 0.01	0.86	0.09	0.36	− 0.09	0.35	− 0.15	0.11
4	IC3	Cerebello-thalamic	− 0.48	3.23e−07*	14	0.14	0.11	0.25	21	0.03
5	IC18	Cinguloinsular	− 0.06	0.53	0.11	0.24	− 0.27	0.006	− 0.07	0.46
6	IC15	Thalamic	− 0.29	0.002	0.48	2.71e−07*	− 0.06	0.95	0.24	0.01
7	IC23	Medial-visual	− 0.53	1.12e−08*	0.15	0.13	0.08	42	0.14	0.13
8	IC19	Perisylvian	− 0.01	0.99	− 0.01	0.85	0.53	1.5e−08*	0.19	0.04
9	IC25	Superior frontal	− 0.07	0.48	0.04	0.62	0.11	0.26	0.07	0.46
10	IC32	Temporo-thalamic	− 0.03	0.75	− 0.11	0.24	0.31	0.0016	− 0.01	0.99

* p values indicate network strength significantly correlated with clinical features and survive after FDR correction

epileptic drugs indicating a "hyper-connected plasticity" response in the brain proportional to the disease [38]. Progressive atrophy of hippocampus is a well-known finding in patients with MTS and the negative correlation of the posterior quadrant (IC 12) and temporo-thalamic networks (IC 32) with hippocampal volume gives direct evidence of the recruitment of these areas with progressive loss of hippocampal volume. The absence of a correlation with unaffected hippocampal size in the same patients also further supports the epilepsy specific nature of these networks. Clinically earlier age at onset, increased duration of epilepsy, higher frequency of seizure, and a requirement for the higher number of drugs of seizure control are often implicated in "epileptogenesis" indicating disease progression [39]. In patients with temporal lobe epilepsy (TLE), it is now known that various factors including genes, environment, and neuronal plasticity can continue to alter the brain by a process called "epileptogenesis." It is an evolving process and the seizures that we see clinically are superimposed on this epileptogenic brain, making epilepsy a complex disease with diverse clinical and electrophysiological features [40]. Simulated neuronal models using rsfMRI on rat dentate gyrus have revealed hyperconnectivity response with an increased small-worldness of the network (increase in path length and clustering coefficient), in the early stage of the disease with a rapid reduction in path length associated with near total loss of hilar neurons [41] supporting epileptogenesis can be measured in vivo. Based on these evidences, we speculate that the observation of network hyperconnectivity with disease progression found in our study could be indicative of "epileptogenesis." However, longitudinal studies in patients with different kinds of epilepsy, and its correlation with post-operative seizure freedom will further throw light on the predictive relevance of this observation.

It is interesting to note that the 97.52% accuracy of SVM is higher than reported interictal scalp EEG sensitivity of 80–90% [42]. However, since the detection of interictal discharges depends on several factors including seizure frequency, sleep deprivation, type of epilepsy, medications, and inter-observer variability, the sensitivity of scalp EEG is highly variable [43]. Complimentary methods like automated spike detection have increased the sensitivity of IED by reducing the inter-observer variability [44]. Prior imaging studies using SVM also have revealed accuracies up to 93% with anatomical data and DTI as inputs in the diagnosis of TLE [45] and up to 95% using rsfMRI graph in the lateralisation of TLE [46]. Apart from comparable accuracy in the current study using rsfMRI, a notable point is the report of the anatomy top 10 networks using the elastic net. Objective visualization of these networks apart from the assisting in the diagnosis of disease, if found valid in future studies, could also assist in tracking its progression in the period prior to the onset of refractory seizures.

It needs to be noted that, since this was an exploratory study, we only considered the top ranking 10 networks. Even among these ten, some of the ICs (IC 10, 22, 18, 25) did not reveal significant correlations with clinical features. We presume the lack of clinical correlation could be because the clinical features that we had in hand were few and might not be reflective of epilepsy and epileptogenesis in its entirety. Objective capture of seizure semiology, electrophysiological spread during ictus, and nature of interictal discharges could help in further characterizing these epilepsy networks. The method of hand classification of ICA, though has its own advantages, its replicability needs further validation. Comparative studies using automated classification methods like FSL-FIX and ICA-AROMA might provide additional inputs. It also needs to be noted that the patients belonged to the drug-resistant TLE and hence, the application of these findings to recent onset epilepsy and extra-temporal and generalized epilepsies needs further validation. Correlation of these networks with the neuropsychological scores would have helped us attribute changes to disease/drug-dependent effects on cognitive functions.

Despite these limitations, the findings from the current study have advanced literature, as it has introduced the concept of disease induced "rsfMRI epilepsy networks." Though the evidence is not as compelling as the imaging evidence of hippocampal sclerosis in MTS, it is now possible to believe that ICA-derived resting-state networks, apart from providing important information with regard to brain function, also carries relevant information about diseases and in future could be important markers in heterogeneous diseases like epilepsy.

Conclusion

The findings from the current study have provided proof of concept evidence for rsfMRI epilepsy networks. It is now possible to believe that ICA networks could also carry disease-sensitive information about epilepsy.

Compliance with ethical standards

Conflict of interest The authors of this manuscript declare no relationships with any companies whose products or services may be related to the subject matter of the article.

Statistics and biometry One of the authors has significant statistical expertise.

Informed consent Written informed consent was obtained from all subjects (patients) in this study.

Ethical approval Institutional Review Board approval was obtained.

Methodology
• Prospective
• Case-control study
• Performed at one institution

Publisher's note Springer Nature remains neutral with regard to jurisdictional claims in published maps and institutional affiliations.

References

1. Chiang S, Haneef Z (2014) Graph theory findings in the pathophysiology of temporal lobe epilepsy. Clin Neurophysiol 125:1295–1305
2. Liao W, Zhang Z, Pan Z et al (2010) Altered functional connectivity and small-world in mesial temporal lobe epilepsy. PLoS One 5:e8525
3. Vlooswijk MC, Vaessen MJ, Jansen JF et al (2011) Loss of network efficiency associated with cognitive decline in chronic epilepsy. Neurology 77:938–944
4. Liao W, Zhang Z, Pan Z et al (2011) Default mode network abnormalities in mesial temporal lobe epilepsy: a study combining fMRI and DTI. Hum Brain Mapp 32:883–895
5. Widjaja E, Zamyadi M, Raybaud C, Snead OC, Smith ML (2013) Abnormal functional network connectivity among resting-state networks in children with frontal lobe epilepsy. AJNR Am J Neuroradiol 34:2386–2392
6. Zhang Z, Lu G, Zhong Y et al (2009) Impaired perceptual networks in temporal lobe epilepsy revealed by resting fMRI. J Neurol 256:1705–1713
7. Waites AB, Briellmann RS, Saling MM, Abbott DF, Jackson GD (2006) Functional connectivity networks are disrupted in left temporal lobe epilepsy. Ann Neurol 59:335–343
8. Luo C, Li Q, Xia Y et al (2012) Resting state basal ganglia network in idiopathic generalized epilepsy. Hum Brain Mapp 33:1279–1294
9. Damoiseaux JS, Rombouts SA, Barkhof F et al (2006) Consistent resting-state networks across healthy subjects. Proc Natl Acad Sci U S A 103:13848–13853
10. Beckmann CF, Smith SM (2005) Tensorial extensions of independent component analysis for multisubject FMRI analysis. Neuroimage 25:294–311
11. Smith SM, Jenkinson M, Woolrich MW et al (2004) Advances in functional and structural MR image analysis and implementation as FSL. Neuroimage 23(Suppl 1):S208–S219
12. Cerliani L, Thomas RM, Aquino D, Contarino V, Bizzi A (2017) Disentangling subgroups of participants recruiting shared as well as different brain regions for the execution of the verb generation task: a data-driven fMRI study. Cortex 86:247–259
13. Li S, Tian J, Li M et al (2018) Altered resting state connectivity in right side frontoparietal network in primary insomnia patients. Eur Radiol 28:664–672
14. Panda R, Bharath RD, Upadhyay N, Mangalore S, Chennu S, Rao SL (2016) Temporal dynamics of the default mode network characterize meditation-induced alterations in consciousness. Front Hum Neurosci 10:372
15. Schölvinck ML, Maier A, Ye FQ, Duyn JH, Leopold DA (2010) Neural basis of global resting-state fMRI activity. Proc Natl Acad Sci U S A 107:10238–10243
16. Rodionov R, De Martino F, Laufs H et al (2007) Independent component analysis of interictal fMRI in focal epilepsy: comparison with general linear model-based EEG-correlated fMRI. Neuroimage 38:488–500
17. Simon P (2013) Too big to ignore: the business case for big data. John Wiley & Sons, Inc. New Jersey
18. Arbabshirani MR, Plis S, Sui J, Calhoun VD (2017) Single subject prediction of brain disorders in neuroimaging: promises and pitfalls. Neuroimage 145:137–165
19. Tognin S, Pettersson-Yeo W, Valli I et al (2013) Using structural neuroimaging to make quantitative predictions of symptom progression in individuals at ultra-high risk for psychosis. Front Psychiatry 4:187
20. van der Burgh HK, Schmidt R, Westeneng HJ, de Reus MA, van den Berg LH, van den Heuvel MP (2017) Deep learning predictions of survival based on MRI in amyotrophic lateral sclerosis. Neuroimage Clin 13:361–369
21. Chen CP, Keown CL, Jahedi A et al (2015) Diagnostic classification of intrinsic functional connectivity highlights somatosensory, default mode, and visual regions in autism. Neuroimage Clin 8:238–245
22. Kaufmann T, Skåtun KC, Alnaes D et al (2015) Disintegration of sensorimotor brain networks in schizophrenia. Schizophr Bull 41:1326–1335
23. Ryali S, Chen T, Supekar K, Menon V (2012) Estimation of functional connectivity in fMRI data using stability selection-based sparse partial correlation with elastic net penalty. Neuroimage 59:3852–3861
24. Ng B, Vahdat A, Hamarneh G, Abugharbieh R (2010) Generalized sparse classifiers for decoding cognitive states in fMRI. In: Wang F, Yan P, Suzuki K, Shen D (eds) Machine Learning in Medical Imaging. Lecture Notes in Computer Science, vol 6357. Springer, Berlin
25. Sochat V, Supekar K, Bustillo J, Calhoun V, Turner JA, Rubin DL (2014) A robust classifier to distinguish noise from fMRI independent components. PLoS One 9:e95493
26. Beckmann CF, DeLuca M, Devlin JT, Smith SM (2005) Investigations into resting-state connectivity using independent component analysis. Philos Trans R Soc Lond Ser B Biol Sci 360:1001–1013
27. Beckmann CF, Mackay CE, Filippini N, Smith SM (2009) Group comparison of resting-state FMRI data using multi-subject ICA and dual regression. Neuroimage 47:S148
28. Chollet F (2015) Keras: deep learning library for theano and tensorflow. Available via https://keras.io
29. Zou H, Hastie T (2005) Regularization and variable selection via the elastic net. J R Statist Soc B 67:301–320
30. Barrat A, Barthélemy M, Pastor-Satorras R, Vespignani A (2004) The architecture of complex weighted networks. Proc Natl Acad Sci U S A 101:3747–3752
31. Suppa P, Anker U, Spies L et al (2015) Fully automated atlas-based hippocampal volumetry for detection of Alzheimer's disease in a memory clinic setting. J Alzheimers Dis 44:183–193
32. Eickhoff SB, Stephan KE, Mohlberg H et al (2005) A new SPM toolbox for combining probabilistic cytoarchitectonic maps and functional imaging data. Neuroimage 25:1325–1335
33. Smith SM, Fox PT, Miller KL et al (2009) Correspondence of the brain's functional architecture during activation and rest. Proc Natl Acad Sci U S A 106:13040–13045
34. Barba C, Rheims S, Minotti L et al (2016) Reply: temporal plus epilepsy is a major determinant of temporal lobe surgery failures. Brain 139:e36

35. Kelly RE Jr, Alexopoulos GS, Wang Z et al (2010) Visual inspection of independent components: defining a procedure for artifact removal from fMRI data. J Neurosci Methods 189:233–245

36. Griffanti L, Douaud G, Bijsterbosch J et al (2017) Hand classification of fMRI ICA noise components. Neuroimage 154:188–205

37. Feigin A, Kaplitt MG, Tang C et al (2007) Modulation of metabolic brain networks after subthalamic gene therapy for Parkinson's disease. Proc Natl Acad Sci U S A 104:19559–19564

38. Hillary FG, Rajtmajer SM, Roman CA et al (2014) The rich get richer: brain injury elicits hyperconnectivity in core subnetworks. PLoS One 9:e104021

39. Pitkänen A, Sutula TP (2002) Is epilepsy a progressive disorder? Prospects for new therapeutic approaches in temporal-lobe epilepsy. Lancet Neurol 1:173–181

40. Scharfman HE (2007) The neurobiology of epilepsy. Curr Neurol Neurosci Rep 7:348–354

41. Dyhrfjeld-Johnsen J, Santhakumar V, Morgan RJ, Huerta R, Tsimring L, Soltesz I (2007) Topological determinants of epileptogenesis in large-scale structural and functional models of the dentate gyrus derived from experimental data. J Neurophysiol 97:1566–1587

42. Salinsky M, Kanter R, Dasheiff RM (1987) Effectiveness of multiple EEGs in supporting the diagnosis of epilepsy: an operational curve. Epilepsia 28:331–334

43. Javidan M (2012) Electroencephalography in mesial temporal lobe epilepsy: a review. Epilepsy Res Treat 2012:637430

44. Fergus P, Hussain A, Hignett D, Al-Jumeily D, Abdel-Aziz K, Hamdan H (2016) A machine learning system for automated whole-brain seizure detection. Appl Comput Inf 12:70–89

45. Focke NK, Yogarajah M, Symms MR, Gruber O, Paulus W, Duncan JS (2012) Automated MR image classification in temporal lobe epilepsy. Neuroimage 59:356–362

46. Chiang S, Levin HS, Haneef Z (2015) Computer-automated focus lateralization of temporal lobe epilepsy using fMRI. J Magn Reson Imaging 41:1689–1694

Affiliations

Rose Dawn Bharath [1,2] · Rajanikant Panda [1,2,3] · Jeetu Raj [4] · Sujas Bhardwaj [1,2,5] · Sanjib Sinha [5] · Ganne Chaitanya [5,6] · Kenchaiah Raghavendra [5] · Ravindranadh C. Mundlamuri [5] · Arivazhagan Arimappamagan [7] · Malla Bhaskara Rao [7] · Jamuna Rajeshwaran [8] · Kandavel Thennarasu [9] · Kaushik K. Majumdar [10] · Parthasarthy Satishchandra [7] · Tapan K. Gandhi [11]

1. Neuroimaging and Interventional Radiology, National Institute of Mental Health and Neuro Sciences, Bangalore, Karnataka 560029, India

2. Advance Brain Imaging Facility, Cognitive Neuroscience Centre, National Institute of Mental Health and Neuro Sciences, Bangalore, Karnataka 560029, India

3. Coma Science Group, GIGA-Consciousness, Universitè de Liège, Liège, Belgium

4. Department of Computer Science, Indian Institute of Technology Delhi, New Delhi, Delhi 110016, India

5. Neurology, National Institute of Mental Health and Neuro Sciences, Bangalore, Karnataka 560029, India

6. Department of Neurology, Thomas Jefferson University, Philadelphia, PA, USA

7. Neurosurgery, National Institute of Mental Health and Neuro Sciences, Bangalore, Karnataka 560029, India

8. Neuropsychology, National Institute of Mental Health and Neuro Sciences, Bangalore, Karnataka 560029, India

9. Biostatistics, National Institute of Mental Health and Neuro Sciences, Bangalore, Karnataka 560029, India

10. Systems Science and Informatics Unit, Indian Statistical Institute, Bangalore, Karnataka 560059, India

11. Department of Electrical Engineering, Indian Institute of Technology Delhi, (IIT-D), New Delhi, Delhi 110016, India